Responses of the hydrological cycle to solar forcings

Jane Smyth

Advised by Dr. Trude Storelvmo
Second Reader Dr. William Boos
May 6, 2016

A Senior Thesis presented to the faculty of the Department of Geology and Geophysics, Yale University, in partial fulfillment of the Bachelor's Degree.

RESPONSES OF THE HYDROLOGICAL CYCLE TO SOLAR FORCINGS

JANE SMYTH

ADVISED BY DR. TRUDE STORELVMO

Senior Thesis

CONTENTS

Department of Geology & Geophysics, Yale University, New Haven, Connecticut

OVERVIEW

The relationship between sunlight and rainfall is fundamental to the Earth's climate. This thesis studies how perturbations to the incoming solar radiation affect precipitation patterns in a series of experiments using global climate models (GCMs). The first chapter describes a study of the thermodynamic and dynamic responses of the hydrological cycle to a simplified representation of solar geoengineering in a suite of twelve GCMs. In each model of the Geoengineering Modeling Intercomparison Project (GeoMIP), atmospheric carbon dioxide levels are quadrupled, and the solar constant is reduced uniformly in time and space, dimming the planet and largely restoring preindustrial temperatures. We attribute simulated rainfall anomalies between this solar dimming experiment and the preindustrial control to a combination of mechanisms: the thermodynamic scaling of net precipitation, relative humidity fluctuations, and shifts of the Hadley circulation.

The second chapter presents a study of the influence of Holocene orbital parameters on regional and zonal mean precipitation patterns, with a focus on the West African monsoon. We analyze simulations of a natural alteration of the distribution of sunlight, which varies seasonally and across latitudes, in a single climate model (Geophysical Fluid Dynamics Laboratory AM2.1). In both chapters, an energetic perspective relates the given radiative perturbation to rainfall and underlying atmospheric dynamics.

1 CHAPTER I: SOLAR GEOENGINEERING

1.1 Abstract

The primacy of the hydrological cycle in global climate motivates thorough evaluation of its responses to climate change and mitigation. The Geoengineering Model Intercomparison Project (GeoMIP) is a global collaboration that aims to assess the climate impacts of solar geoengineering, a proposal to counteract global warming with a reduction of incoming solar radiation. We assess the mechanisms underlying the rainfall response to a simplified simulation of solar dimming in twelve GeoMIP model experiments and identify robust features. While solar geoengineering restores preindustrial temperatures, the global hydrology is altered. Tropical precipitation changes dominate the response across the model suite. The models indicate a range of possibilities for the hydrological response, and in most cases, both thermodynamic and non-thermodynamic mechanisms drive net precipitation changes in the geoengineered simulations relative to the preindustrial. Changes in relative humidity and shifts of the Hadley circulation cells cause greater rainfall changes than the Clausius-Clapeyron scaling of net precipitation. The variations among models in the movement of crucial tropical rainfall bands highlights the need for cautious consideration and continued study before any implementation of solar geoengineering.

KEYWORDS Hydrological cycle, geoengineering, Hadley circulation, thermodynamic scaling

1.2 Introduction

1.2.1 *Solar Geoengineering*

Solar geoengineering has been suggested as a way to counter the effects of global warming induced by anthropogenic greenhouse gas emissions (Robock et al. 2009). By reducing incoming solar radiation, solar geoengineering would bring the climate with elevated concentrations of CO2 into radiative balance. It compensates for a change in surface temperature from longwave trapping with a reduction of incoming shortwave radiation. Solar geoengineering is a controversial proposal, but should it come into favor due to continued greenhouse gas emissions, it is critical that the climate effects be understood before deployment (NRC 2015).

The Geoengineering Model Intercomparison Project (GeoMIP) is intended to determine robust responses of the climate to various simulations of solar geoengineering, in experiments that range from simple representations of the solar dimming, to realistic representations of stratospheric aerosol emissions (Kravitz et al. 2010). The GeoMIP experiments are based on the Coupled Model Intercomparison Project Phase Five (CMIP5), which is a protocol to study the output of coupled atmosphere-ocean climate models. Twelve fully coupled models participated in the G1 experiment, and they differ in their ocean, ice sheet, land surface and atmospheric components. The latter two components are particularly relevant for this study. All of the models except EC-Earth include the CO2 physiological effect, whereby plant stomata constrict in environments with high ambient CO2, reducing evapotranspiration (Irvine et al. 2014). Some, but not all models, feature dynamic vegetation distributions (Table 3 on page 16). The twelve models include a wide range of parametrizations and configurations, allowing for strong conclusions about robust climate responses that appear across models (Kravitz et al. 2013a).

The GeoMIP G1 experiment counteracts the forcing from quadrupled atmospheric CO_2 levels with a simple reduction of the solar constant. The idealized nature of this simulation is conducive to multimodel comparison. It superimposes two large and opposite climate forcings, which offset one another nearly completely in terms of global mean net radiation balance at the top of the atmosphere and near-surface atmospheric temperature, but that do not totally cancel in their hydrological effects, especially on local scales (Kravitz et al. 2013b).

1.2.2 *The Hydrological Cycle*

The water cycle impacts agriculture, economies, as well as the welfare of ecosystems and human civilizations (IPCC 2014). It is imperative to understand the effects of solar radiation management on global hydrology, to evaluate whether such an approach to climate change mitigation is feasible or desirable.

THERMODYNAMICS Surface heating increases the temperature and the evaporation rate, which increases the atmospheric moisture content, or specific humidity q (Trenberth 1999). we have confidence about certain aspects of the hydrological cycle's response to greenhouse gas warming, particularly those tightly coupled to the increase in saturation vapor pressure with warming (Held and Soden 2006). The Clausius-Clapeyron expression (1 on the next page), where R is the gas constant and L the latent heat of vapor-

ization, relates the derivative of the natural log of saturation vapor pressure e_s with respect to temperature to temperature itself. At typical near-surface temperatures, saturation vapor pressure increases 7% K^{-1}.

$$\frac{d \ln e_s}{dT} = \frac{L}{RT^2} \equiv \alpha(T) \tag{1}$$

Precipitation minus evaporation (P-E), or net precipitation, determines the amount of runoff on land, and the salinity of the water column over ocean. Precipitation minus evaporation follows Clausius-Clapeyron scaling, as in (2), given two important assumptions (Held and Soden 2006). First, the relationship assumes no change in near-surface relative humidity (the ratio of actual vapor pressure to saturation vapor pressure) between climate states. Second, it assumes that there is no change in the atmospheric flow. This thermodynamic scaling equation represents the component of net precipitation change driven directly by surface temperature perturbations. Net precipitation changes not captured by this scaling are driven by non-thermodynamic mechanisms, including changes in relative humidity or atmospheric dynamics.

$$\delta(P - E) = \alpha \, \delta T \, (P - E) \tag{2}$$

This project evaluates the extent to which the basic physical relation between saturation vapor pressure and temperature estimates the climate response to a combination of large-magnitude forcings: greenhouse gas warming and solar dimming.

DYNAMICS Large-scale meridional circulations are driven by energy gradients imposed by the uneven distribution of sunlight on Earth (Schneider et al. 2014). The Hadley circulation cells are responsible for most of the poleward heat transport in the tropics, where the annual solar input is highest (Hill et al. 2015). The net energy flux of the Hadley circulation is in the flow direction of its upper branch (Held 2001). The ascending motion of the Hadley cell drives the seasonally-migrating tropical rainfall known as the Intertropical Convergence Zone (ITCZ), and there is evidence that its position is determined by meridional gradients in the vertically-integrated atmospheric energy budget (Shekhar and Boos 2016). The Hadley circulation is crucial for balancing global energy, so high-latitude temperature anomalies can drive shifts of the ITCZ (Yoshimori and Brocolli 2008). The ITCZ is sensitive to interhemispheric energy contrasts set up by aerosols, clouds, or antisymmetric heating (Seo et al. 2014). A thorough analysis of Hadley circulation changes is a crucial outstanding task for understanding the hydrological response to solar geoengineering (Kravitz et al. 2013b). The meridional streamfunction is derived from the continuity equation, and either v or w can be used to fully define the two-dimensional, overturning flow (3).

$$\Psi(\phi, p) = 2\pi a \cos\phi \int_0^p \bar{v} \, dp/g. \tag{3}$$

Solar radiation management effectively alters the planetary albedo, or the ratio of reflected to incoming solar radiation at the top of the atmosphere. Planetary albedo is a function of clouds, water vapor, ice, snow and vegetation (Voigt and Stevens 2014). As an emergent feature of the system, it varies between models. Satellite observations demonstrate that the Northern and Southern hemispheres have virtually equal albedos, despite the uneven global distribution of land (Voigt et al. 2013). Climate models

fail to reproduce this symmetry in hemispheric albedo, and the consequent meridional albedo structure could alter atmosphere and ocean circulations (Stephens et al. 2015; Donohoe and Battisti 2011). Solar dimming superimposes an effective increase in albedo on an existing meridional albedo profile. This could affect the position of the temperature maximum and thus the location of the ITCZ and precipitation (Haywood et al. 2013). We investigate the possibility of a model's preindustrial hemispheric albedo contrast serving as a predictor of the direction of the Hadley circulation shift with solar geoengineering. In G1, insolation is uniformly reduced at all latitudes, and causes a greater reduction in incoming energy in the hemisphere with the lower preindustrial albedo, according to (4) where E is the energy received, α is the planetary albedo, and I the insolation. In G1, this might lead to a shift of the ITCZ towards the high-albedo hemisphere, since this hemisphere's energy input will be relatively higher.

$$E = (1 - \alpha) * I \tag{4}$$

RELATIVE HUMIDITY Relative humidity is the ratio of actual vapor pressure to saturation vapor ($\frac{e}{e_s}$), or almost equivalently, specific humidity to saturation specific humidity ($\frac{q}{q_s}$) (Peixoto and Oort 1996). It can change with the evaporation rate or temperature, with the latter affecting the saturation vapor pressure as in (1 on the previous page) (Peixoto and Oort 1996). The assumption of constant relative humidity in the thermodynamic scaling of P-E relies on the availability of moisture. In a moisture-limited regime (i.e. over land) the specific humidity q may not increase proportionally with temperature, breaking the assumption of constant relative humidity. Under this circumstance, relative humidity adjustments would contribute to non-thermodynamic changes in the P-E between climate states. The relative humidity parameter is also of interest in climate change studies for evaluating the risk of human heat stress, under both high and low RH extremes (Sherwood and Huber 2010; Souch and Grimmond 2004).

1.3 Models & Methods

The GeoMIP model suite (Table 1 on the following page) followed a protocol for the preindustrial (PiCon), global warming (abrupt4xCO2), and geoengineered (G1) climate simulations. Preindustrial control simulations (CMIP5 3.1) were run for 500 years after model spin-up, with preindustrial land cover and atmospheric compositions (Kravitz et al. 2010). Abrupt4xCO2 simulations were run with a quadrupling of carbon dioxide from the preindustrial control, and were run for 150 years. The G1 scenario simulates a uniform and instantaneous dimming of the solar constant across all wavelengths and spectra. The G1 experiment was run from the steady state preindustrial control run, followed by an abrupt quadrupling of CO_2, and a simultaneous solar constant reduction for 50 years, plus an optional 20 year cessation period. Some of the later GeoMIP experiments simulate the injection of sulfate stratospheric aerosols, but this study only considers the G1 experiment.

As some small top of the atmosphere (TOA) net radiation anomaly is expected in the preindustrial control run, the geoengineered scenario TOA radiation balance is expected to fall within 0.1 W m^{-2} of the control run net radiation balance (Kravitz et al. 2010). The steady state difference in radiation between the quadrupled CO2 run and the preindustrial control is

Table 1: GeoMIP Suite. Resolution given either in degrees or number of boxes (lat x lon), or in number of spectral elements (T)/number of vertical layers (L). Information courtesy of Kravitz et al. 2013a

Model[1]	Atmosphere Res.	Ocean Res.
BNU-ESM	T42/L26	200 x 360 boxes
Can-ESM2	T63/L35	0.94 x 1.4/L40
CESM-CAM5.1-FV	1.9 x 2.5/L30	1 x 1/L60
CCSM4	0.9 x 1.25/L28	1 x 1/L60
EC-Earth	T159/L62	1 x 1/L42
GISS-E2-R	2 x 2.5/L40	1 x 1.25/L32
HadCM3	2.5 x 3.75/L19	1.25 x 1.25/L20
HadGEM2-ES	1.25 x 1.875/L38	1/3-1 x 1/L40
IPSL-CM5A-LR	2.5 x 3.75/L39	96 x 95 boxes/L39
MIROC-ESM	T42/L80	0.5-1.4 x 1.4/L44
MPI-ESM-LR	T63/L47	1.5 x 1.5/L40
NorESM1-M	1.9 x 2.5/L26	1 x 1/L70

1. **Full Names:** BNU-ESM, Beijing Normal University-Earth System Model; CanESM2, The Second Generation Canadian Earth System Model; CESM-CAM5.1, The Community Climate System Model Version 5.1; CCSM4, The Community Climate System Model Version 4; EC-EARTH DMI, European Earth System Model based on ECMWF Models (Seasonal Forecast System), Danish Meteorological Institute; GISS-E2-R, Goddard Institute for Space Studies ModelE version 2; HadCM3, Hadley Centre coupled model 3; IPSL-CM5A-LR, Institut Pierre Simon Laplace ESM; MIROC-ESM, Model for Interdisciplinary Research on Climate-Earth System Model; MPI-ESM-LR, Max Planck Institute ESM; NorESM1-M, Norwegian ESM.

used to solve for the value of the solar constant to be used in a particular model group's G1 simulation, according to (5), where RF is the radiative forcing, S_0 is the solar constant, and α is the planetary albedo. The value of the solar radiation reduction is adjusted by each model group to achieve TOA radiation balance within the specified range during the first ten years of the run.

$$\Delta RF = S_0\, 4(1-\alpha) \tag{5}$$

We investigate how well thermodynamic scaling predicts hydrologic changes in a geoengineered climate for each model by comparing the prediction using (2 on page 6) to the annual and zonal mean net precipitation anomaly between G1 and the Preindustrial climate in the model simulations. We also consider the annual-mean global distribution of precipitation minus evaporation anomalies.

To discern the component of the precipitation change caused by changes in large scale atmospheric dynamics, we calculated the change in the Hadley circulation between the G1 and Preindustrial Control simulations. For each model, we calculated the meridional streamfunction over a 50 year averaging period based on the modeled meridional wind vector, v 10 on page 26. We calculated annual and seasonal mean dynamical changes to analyze the changes in the zonal mean hydrological cycle. We calculated the planetary albedo in the preindustrial simulation of each model to better interpret the dynamical changes, if any. We computed area-weighted hemispheric averages as the ratio of reflected to incident shortwave radiation at TOA, averaged over a 50 year period.

We consider the absolute changes in the relative humidity distribution to explain precipitation anomalies between G1 and the preindustrial simulations unaccounted for by thermodynamic or dynamic mechanisms.

The relative humidity and streamfunction analyses are complete for a subset of the ensemble, due to limited functionality of the central GeoMIP model data server, the Earth System Grid Federation (ESGF).

1.4 Results and Discussion

The experimental design results in minimal temperature anomalies between G1 and the preindustrial control (Fig. 5 on page 18), but does not eliminate hydrological effects. Figures 6 on page 19 and 7 on page 20, which separate the precipitation and evaporation changes from solar dimming, reveal that most of the spatial structure in the net precipitation anomaly comes from the precipitation change.

1.4.1 *Thermodynamic Scaling of Net Precipitation*

The thermodynamic scaling predicts virtually no change in global net precipitation, since by experimental design the temperature anomaly is minimal between the G1 and preindustrial scenarios. Maps of the temperature anomalies between G1 and the preindustrial control show variations within 1 K, with some residual warming at high latitudes as a robust feature across the suite (Fig. 5 on page 18). This incomplete restoration of polar temperatures is most pronounced in BNU-ESM, where Arctic warming relative to the preindustrial exceeds 2 K. The discrepancies between the thermodynamic scaling and the ensemble mean precipitation result are within 0.2 mm/day, with the most pronounced differences in the tropics however, where temperature anomalies are minimal (Fig 1 on the following page). Previous research has suggested that this is a result of the nature of the G1 experiment forcing. Solar geoengineering might suppress tropical precipitation since solar reduction cools the surface more than the mid-troposphere, increasing atmospheric stability and reducing convection (Bala et al. 2008). However, looking at the zonal patterns for individual models (Fig 2 on page 11), there are stronger hydrological effects that cancel out in the ensemble mean. HadCM3, HadGEM2-ES, and CESM-Cam5.1-FV models show a northward shift in the ITCZ, while GISS-E2-R, Can-ESM2, and to a lesser extent MIROC-ESM, demonstrate a southward shift. Annual mean anomalies in the zonal mean exceed 0.6 mm/day in the GISS-E2-R and HadGEM2-ES simulations. In CCSM4, IPSL-CM5A-LR, and NorESM1-M models, the ITCZ narrows, with precipitation increasing at the equator and decreasing within 10 degrees latitude North and South. The precipitation results of the EC-EARTH model are un-physical.

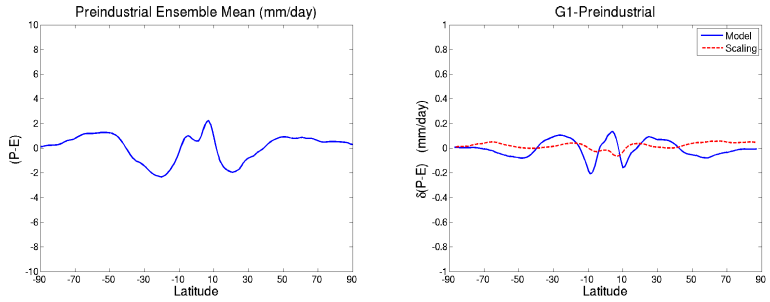

Figure 1: On the left is the ensemble zonal mean net precipitation in the Preindustrial simulation. On the right is the ensemble zonal mean change in precipitation minus evaporation between G1 and the Preindustrial Control. The dashed line is the thermodynamic component, as calculated in (2 on page 6). Both ensembles exclude EC-Earth, which exhibits an unphysical result.

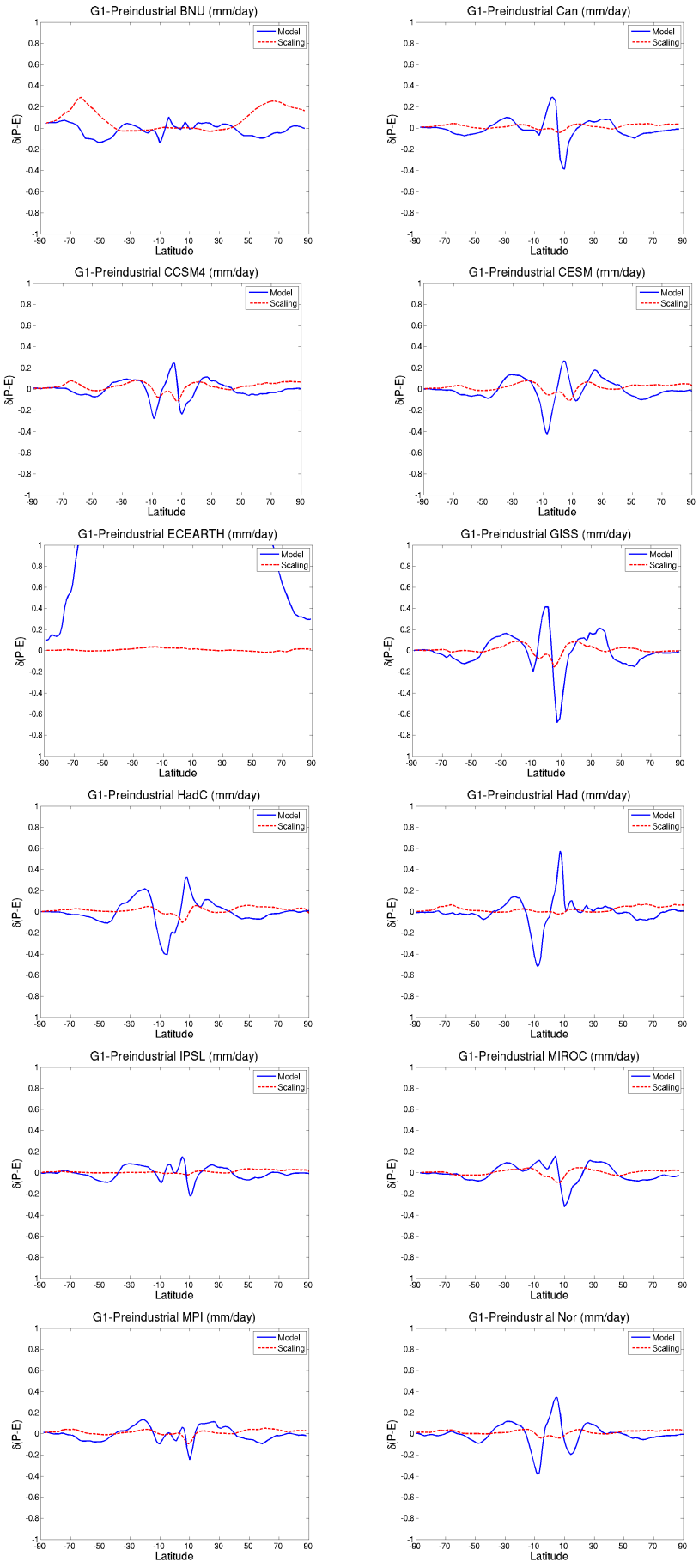

Figure 2: The zonal mean change in precipitation minus evaporation between G1 and the Preindustrial Control. The dashed line is the thermodynamic component, as calculated in 2 on page 6.

1.4.2 *Dynamically Driven Precipitation*

The annual mean Hadley circulation changes vary in magnitude and direction amongst the GeoMIP ensemble members and contribute to dynamic moistening and drying. The meridional streamfunction plots suggest that the ITCZ shifts northward (HadGEM2-ES) and southward (GISS-E2-R, MIROC-ESM), characterized by counterclockwise or clockwise tropical anomalies respectively, are dynamically driven (Fig 3 on the following page). The mean circulation does not seem to provide a dynamical basis for the annual mean constriction of the ITCZ in the MPI and IPSL models, in which anomalies are less than 5 $kgs^{-1} \times 10^9$. Small changes in the latitudinal range and strength of the Hadley circulation and associated precipitation have large local implications, especially on subannual scales (Kang et al. 2009). We find that summer (July-August-September, or JAS) and winter (December-January-February, or DJF) meridional streamfunction anomalies are in every model stronger than the annual mean, since opposite responses in different seasons average out in the annual mean (Fig 8 on page 21). In HadGEM2-ES, for example, the JAS meridional mass flux anomaly exceeds 40 $kgs^{-1} \times 10^9$. On the opposite extreme, the IPSL-CM5A-LR model JAS and DJF mass flux anomalies are below 15 $kgs^{-1} \times 10^9$.

The results do not support the hypothesis that the preindustrial albedo contrast between hemispheres in climate models can be used to predict the direction of an annual mean ITCZ shift with solar dimming. All but two models (IPSL-CM5A-LR and Can-ESM2) have a brighter Northern Hemisphere (Table 2). There is more variation in the dynamical response amongst models than there is in the hemispheric average albedo contrasts. The differences in planetary albedo amongst climate models are due to variability of the atmospheric contribution, related to uncertainties in clouds and aerosols, rather than the surface contribution (Donohoe and Battisti, 2011).

Table 2: Average preindustrial planetary albedo in the Northern and Southern hemispheres. Column 4 is the inter-hemispheric contrast calculated as SH-NH.

Model	NH	SH	Δ
BNU-ESM	0.321	0.308	-0.012
Can-ESM2	0.306	0.315	0.009
CESM-CAM5.1-FV			
CCSM4	0.307	0.307	-1.8E-05
EC-Earth			
GISS-E2-R	0.316	0.298	-0.018
HadCM3			
HadGEM2-ES	0.309	0.297	-0.012
IPSL-CM5A-LR	0.320	0.334	0.015
MIROC-ESM	0.326	0.324	-0.002
MPI-ESM-LR	0.326	0.318	-0.009
NorESM1-M	0.329	0.318	-0.011

1.4.3 *Relative Humidity*

Any changes in relative humidity between G1 and the preindustrial climate are due to changes in evaporation or evapotranspiration, since saturation vapor pressure is maintained along with temperature in G1 (Fig 6 on page 19). Changes in relative humidity drive non-thermodynamic hydrological shifts.

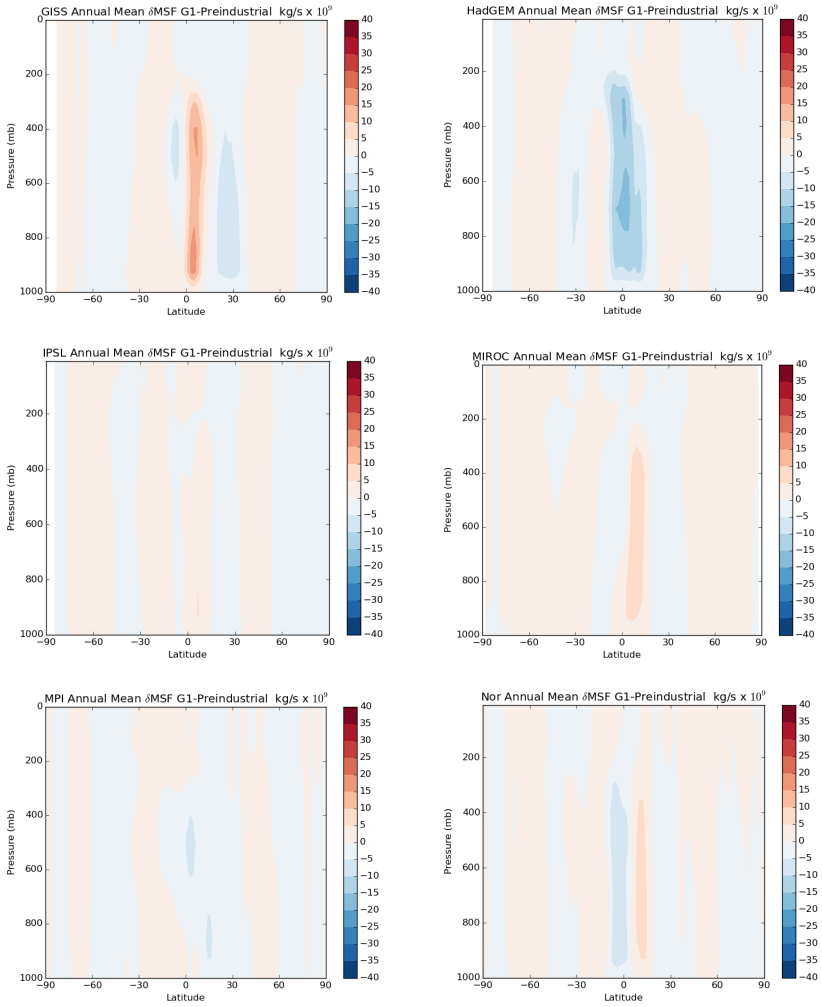

Figure 3: The meridional streamfunction anomaly between G1 and the Preindustrial Control in each model, as calculated in 10 on page 26.

In six of the eight models presented here, relative humidity rates are reduced over land and conserved over ocean (Fig 4 on page 17). The relative humidity reductions are largest over tropical South America and sub-Saharan Africa in the Can-ESM2, CCSM4, GISS-E2-R, HadGEM2-ES, IPSL-CM5A-LR, and NorESM1-M models. The reductions are up to 15% (0.15) in GISS-E2-R and HadGEM2-ES (calculated as the G1 relative humidity (%) minus the Preindustrial relative humidity (%)). The CO_2 physiological effect is included in the land models of eleven GeoMIP simulations, all but EC-Earth (Table 3 on page 16). In response to elevated ambient CO_2 concentrations, plants constrict their stomata, which reduces evapotranspiration in the high CO_2 simulations, including the G1 simulations (Kravitz et al. 2013b). In the abrupt4xCO_2 GeoMIP simulations, this effect is partially offset by the increased net primary productivity in a warmer world. However, in G1, this net primary productivity effect is muted by the reduction in insolation. Tilmes et al. (2013) found that the physiological response to G1 is qualitatively the same as for abrupt4xCO_2. Biogeochemical cycling influences global precipitation as much as the radiative reduction itself (Fyfe et al. 2013).

We consider an additional possible reason for the land-surface contrast in the relative humidity response to solar dimming. Bala et al. (2008) investigate changes in global mean precipitation in a single climate model. They note a greater hydrological sensitivity to solar versus greenhouse forcing and attribute it to global energy budget constraints. Solar forcing heats the surface directly, while greenhouse forcing heats the troposphere. Changes in the insolation therefore have a greater effect on surface net radiation fluxes (i.e., latent and sensible heat fluxes change more than in the CO_2 case). When the downward shortwave flux decreases, the surface fluxes must respond, and in this case the latent heat flux dominates the response. Evaporation decreases, and precipitation follows. Bala et al. do not address how this global mean equilibrium constraint will manifest regionally. It is possible that the pattern we observe of relative humidity changes under geoengineering is a consequence of the climatological relative humidity distribution. There are different starting mean states in relative humidity over land and ocean. Based on observational data, the relative humidity over the ocean is higher than over land in annual and seasonal averages (Peixoto and Oort 1996). This contrast is most apparent at 850 mb, near the surface.

Over ocean the lower atmospheric boundary layer is close to saturation, but cannot exceed 100%. In the geoengineering case, small reductions in evaporation affect the precipitation over ocean, because it means that there is less excess water vapor above the saturation point. In most models, the precipitation response is stronger over ocean than land (Fig 7 on page 20). The relative humidity is constrained because it is still fairly saturated. We do not expect large changes in relative humidity over ocean because evaporation depends on the near-surface relative humidity, which is close to saturation (Byrne and O'Gorman 2013). Since the relative humidity is more constrained over ocean than land, it is consistent that evaporation decreases over land in equilibrium given the energetic processes described by Bala et al. as well as the climatological relative humidity distribution.

1.5 Conclusions

There is not a single mechanism driving the net precipitation changes in climate model simulations of uniform solar dimming. Rather, a combination of thermodynamic scaling of precipitation minus evaporation, relative humidity changes, and Hadley circulation shifts contribute to the hydrological response, to different extents in each model. In the 12-member ensemble, there is variability not only in the spatial distribution of precipitation changes, but also in the underlying causes.

The models can be divided into three groups characterized by different precipitation responses to geoengineering: either a southward shift, northward shift, or narrowing of the ITCZ. Our results support that changes in tropical dynamics, namely shifts of the Hadley circulation, are in part responsible for these alterations to the net precipitation distribution. Previous research documents that Hadley position and strength are influenced by spatial energetic gradients, and that energetic forcing beyond the tropics can cause shifts in the Hadley cell (Schneider et al. 2014). Changes in TOA energy fluxes influence the direction and strength of ITCZ shifts (Kang et al. 2008). Therefore, we hypothesize that these different responses are caused by differences in interhemispheric TOA radiation balance. Our next step is to plot the zonal mean net TOA radiation balance in the preindustrial for each model, as well as the change with solar dimming. This could elu-

cidate what drives the tropical circulation response. We can attribute any apparent intermodel variations in TOA radiation to inconsistent responses by clouds, sea ice, vegetation or other factors depending on the latitude. In a previous study, convection scheme parameters were determinative of the tropical precipitation response to extratropical forcings (Kang et al. 2009). The partitioning of cross-equatorial fluxes between atmospheric and oceanic components is also important for the resulting ITCZ shift, so differences in the oceanic component of the models could emerge as significant (Kang et al. 2008).

We also present evidence that land-sea contrasts in evaporation rates, resulting in land-sea contrasts in relative humidity anomalies, contribute to changes in P-E with solar dimming. We propose that these relative humidity changes could be related to the effect of CO_2 on the stomatal conductance in plants, and to the surface radiative changes necessitated by the solar forcing that are more constrained over ocean than land.

This study demonstrates that tropical precipitation is sensitive to solar perturbations and would be altered by an implementation of solar geoengineering. Based on our inter-model comparison, there is substantial uncertainty regarding the nature of the tropical precipitation response, however, in terms of the direction and strength of the ITCZ shift, as well as its variation on seasonal time scales. Our findings strengthen the conclusion that solar geoengineering cannot restore preindustrial conditions in terms of net precipitation patterns, a fundamental aspect of climate.

1.6 Appendix

Table 3: GeoMIP Model Specifications. Column 3 refers to the CO_2 physiological effect in plants. The S_0 reduction is a percentage. Information courtesy of Kravitz et al. 2013a

Model	Dynamic Vegetation	Phys. Effect	S_0 Reduction
BNU-ESM	no	yes	3.8
Can-ESM2	yes	yes	4.0
CESM-CAM5.1-FV	no	yes	4.7
CCSM4	no	yes	4.1
EC-Earth	N/A	no	4.3
GISS-E2-R	no	yes	4.5
HadCM3	no	yes	4.1
HadGEM2-ES	yes	yes	3.9
IPSL-CM5A-LR	yes	yes	3.5
MIROC-ESM	yes	yes	5.0
MPI-ESM-LR	no	yes	4.7
NorESM1-M	no	yes	4.0

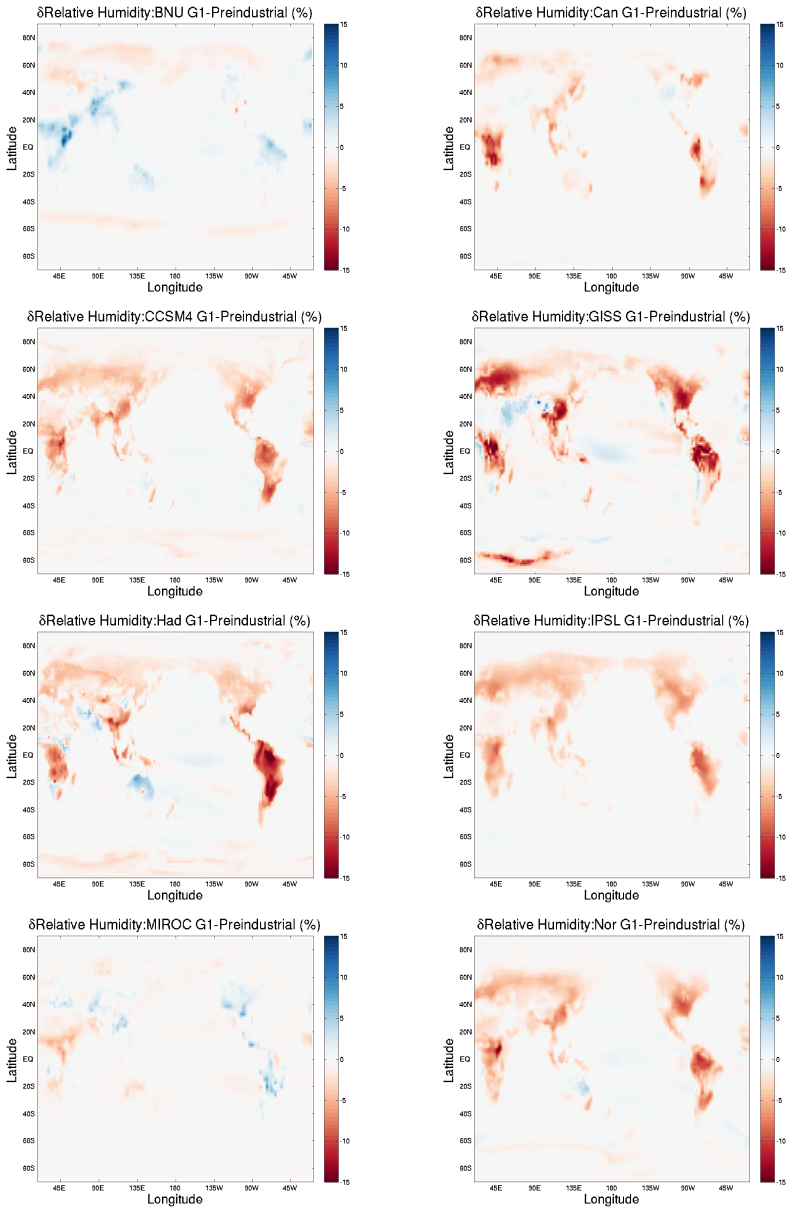

Figure 4: The annual mean near-surface relative humidity anomaly between G1 and the Preindustrial Control in each model.

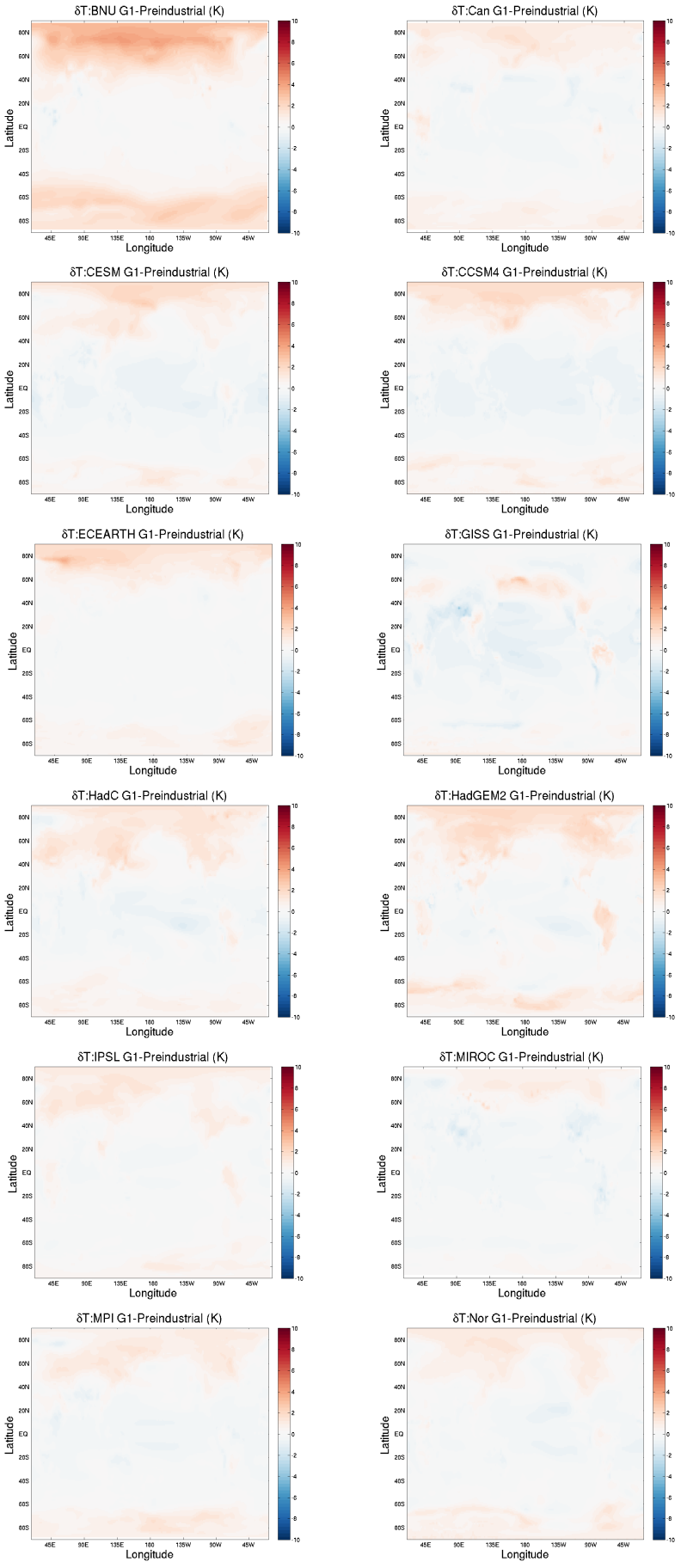

Figure 5: The annual distribution of near-surface atmospheric temperature anomalies (K) between G1 and the Preindustrial Control in each model.

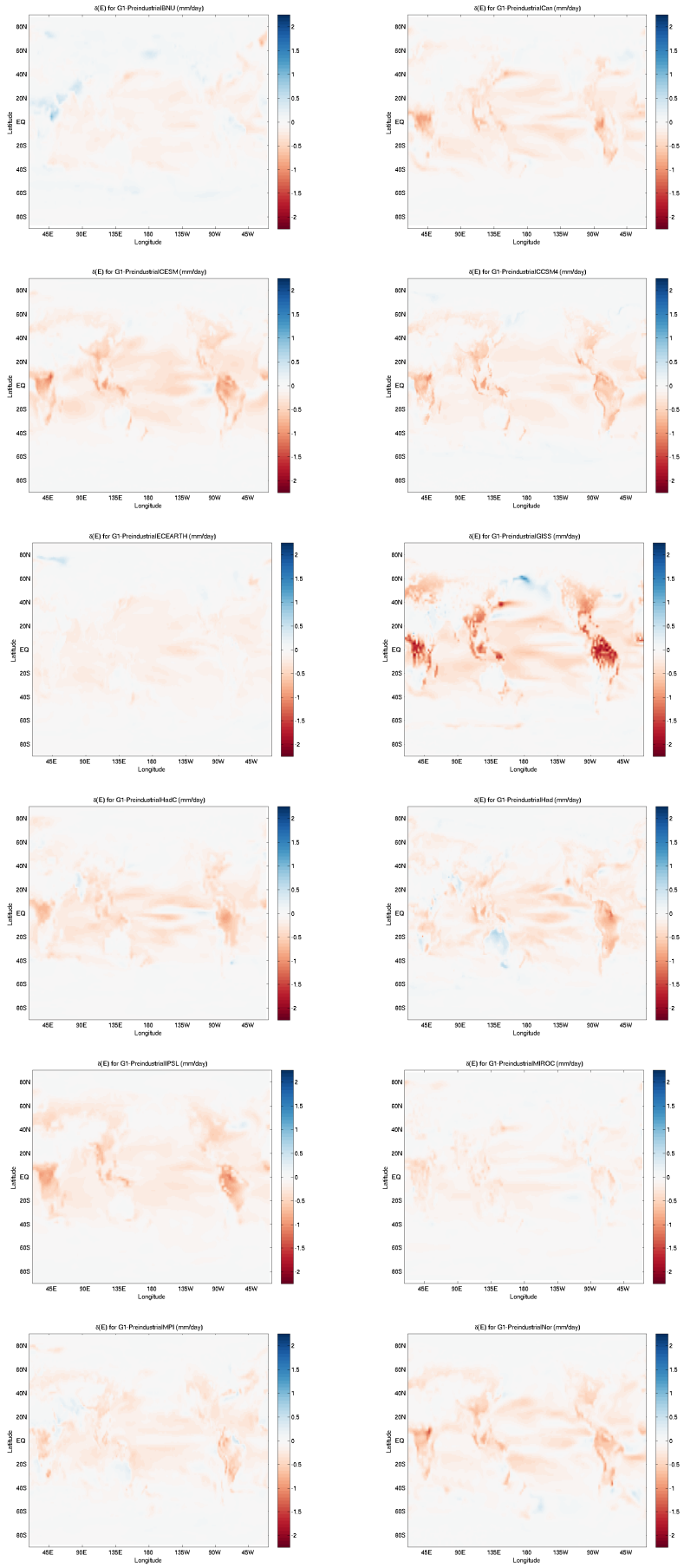

Figure 6: The annual mean distribution of evaporation rate anomalies (mm/year) between G1 and the Preindustrial Control in each model.

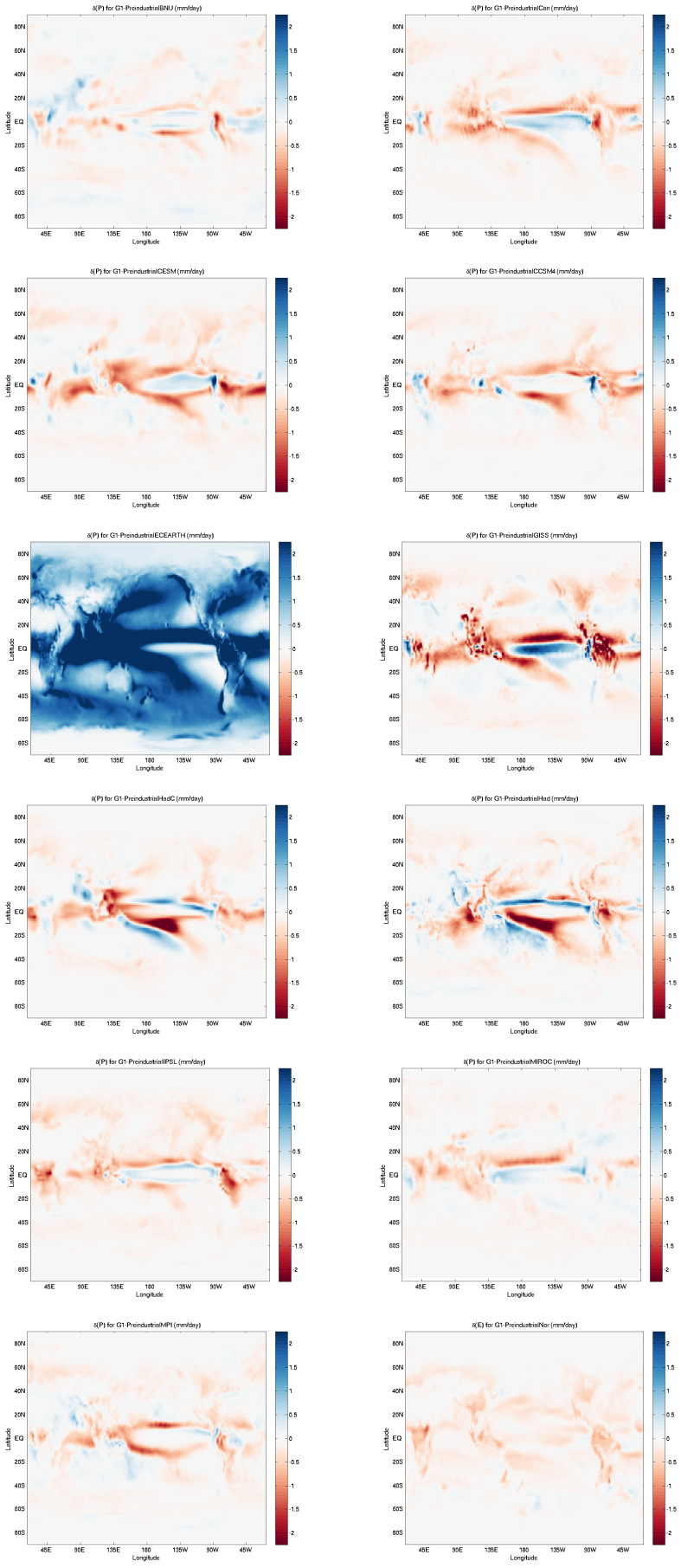

Figure 7: The annual mean distribution of precipitation anomalies (mm/year) between G1 and the Preindustrial Control in each model.

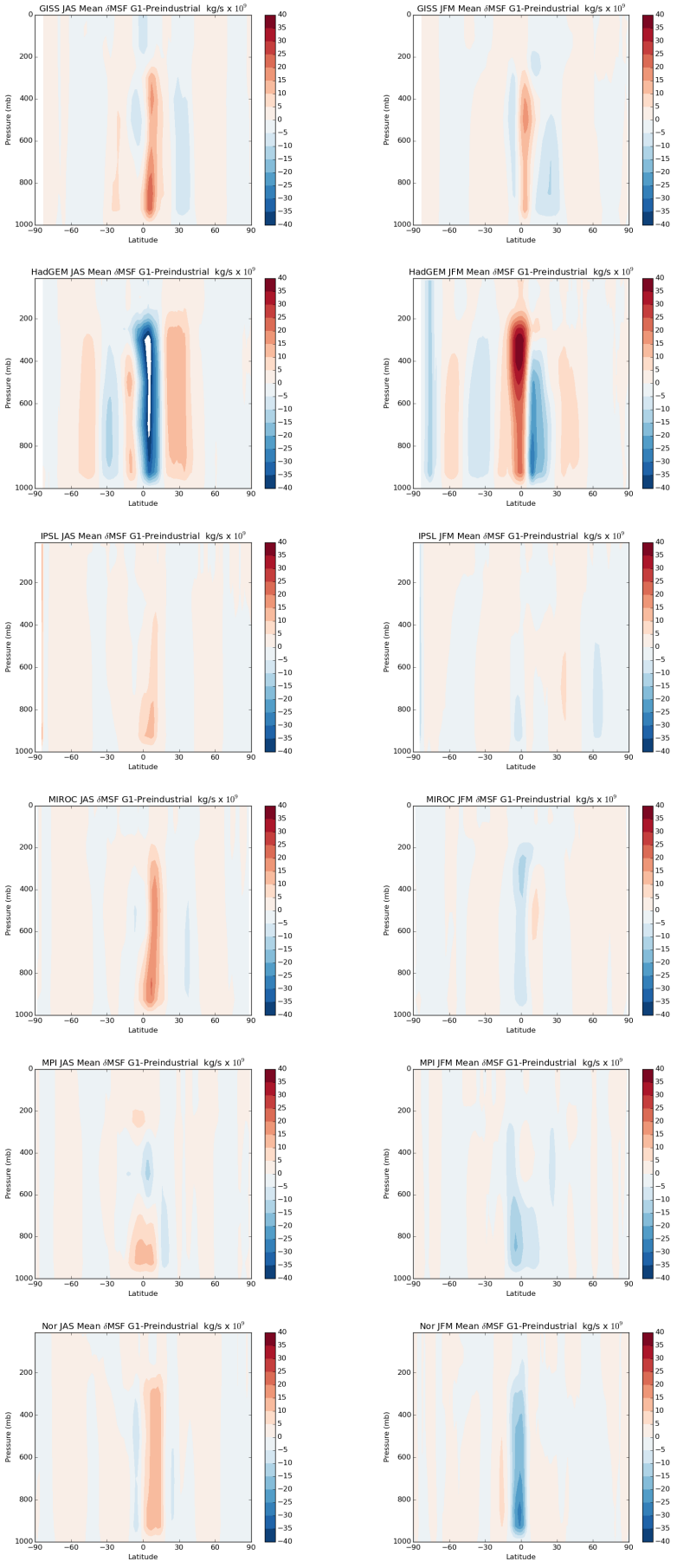

Figure 8: The July-August-September (JAS) and January-February-March (JFM) meridional streamfunction anomalies between G1 and the Preindustrial Control in each model, as calculated in 10 on page 26.

2 CHAPTER II: ORBITAL PRECESSION

Simulated response of the West African monsoon and zonal mean tropical precipitation to Holocene orbital forcing

Advised by Dr. Yi Ming[1] and Spencer Hill[2]

2.1 Abstract

The processes governing West African monsoon variability remain elusive, despite years of sustained scientific research efforts. This study seeks to build a mechanistic understanding of how the insolation changes associated with orbital precession impact the regional and zonal mean tropical precipitation. We isolate the role of sea surface temperature (SST) evolution in modulating the climate response to Holocene orbital precession by considering two sets of atmospheric general circulation model simulations (Geophysical Fluid Dynamics Laboratory AM2.1): one with prescribed SSTs, and one with a 50-meter slab ocean. Model temperature, precipitation, and surface energy budget results confirm the northward migration and intensification of the African monsoon with Holocene precession. This regional response is stronger in the slab ocean experiment, though modest with respect to paleoclimate proxies. The summer zonal mean intertropical convergence zone (ITCZ), however, shifts southward, away from the brighter hemisphere (i.e. the hemisphere which receives more sunlight), with both ocean configurations. This is contrary to what existing theories about the location of the ITCZ predict. The southward energy flux from the high precession summer hemisphere is not accomplished by a stronger Hadley cell mass flux in either experiment; in fact, the circulation weakens in the slab ocean case. The counterintuitive response is attributed to the increase in gross moist stability in the northern tropics in both simulations. The results demonstrate that sea surface temperatures do not fully control the gross moist stability, and that in the zonal mean direction, the tropical circulation response to precession resembles that of an aquaplanet simulation.

Keywords: Precipitation, West African monsoon, Hadley circulation, Paleoclimate

1Geophysical Fluid Dynamics Laboratory,Princeton, New Jersey. **2** *Program in Atmospheric and Oceanic Sciences, Princeton University, Princeton, New Jersey.*

2.2 Introduction

Scientists have approached the question of monsoon variability by simulating the climate of Africa 10,000 years ago (10 ka), during the Holocene Epoch (Patricola and Cook 2007; Braconnot et al. 2000; Liu and Battisti 2015; Bosmans et al. 2012). Ample paleoclimate data indicates that much of Northern Africa was substantially wetter 10 ka than today (Kutzbach and Liu 1997). This was the peak of the African Humid Period (15 to 5 ka), when increased humidity and vegetation characterized the modern Sahara (de Menocal 2015).

The primary orbital signal modulating Holocene radiation was precession, or the wobble of its rotational axis, which has a period of about 20 ka. The Earth's precession was such that the planet was in perihelion during Northern Hemisphere (NH) summer, as opposed to NH winter today. This intensified the NH seasonal cycle in terms of insolation (Fig. 9 on page 25). Precession alters the seasonal distribution of sunlight, but the annual mean insolation at a given latitude is conserved. The obliquity, or axial tilt, was also higher during the Holocene, resulting in slightly reduced annual mean insolation near the equator and enhanced seasonal contrasts at any given latitude (Luan et al. 2012).

The overturning Hadley circulation is driven by the uneven distribution of sunlight on Earth (Hadley, 1735). It dominates the poleward flux of energy in the tropics via its upper branch, whose height and meridional extent are dictated in part by the vertical structure of the atmosphere (Held and Hou 1980). Orbital forcing alters the seasonal distribution of insolation, and thus we expect it to alter the seasonal position and strength of the Hadley cell and the associated precipitation maximum, the Intertropical Convergence Zone (ITCZ). More precisely, we expect the Hadley cell to shift northward and to strengthen in NH summer in the Holocene simulation, to flux anomalous energy southward across the equator (Schneider et al. 2014).

Similarly, monsoons are initiated by moist static energy gradients set up by spatial contrasts in insolation and surface characteristics, and have been understood as seasonal migrations of the ITCZ (Privé and Plumb 2007). Previous research frames monsoons as systems driven by spatial gradients in subcloud thermodynamics, particularly the equivalent potential temperature, a quantity that can characterize the atmosphere over both land and ocean (Hurley and Boos 2013). Therefore, we expect the solar perturbation from orbital precession in atmospheric modeling simulations to influence the position and strength of the West African monsoon. Based on paleoclimate data and past modeling studies, we anticipate that the simulations will show a northward shift and intensification of the West African monsoon with Holocene orbital parameters (Joussame et al. 1999). The mechanisms underlying this system's variability are of great interest, because the African monsoon provides most of the annual precipitation to the Sahel, the transitional zone between the Sahara desert and the Savanna to the south. The Sahel experienced catastrophic droughts between the 1970s and 1990s (Nicholson 2013). A robust theory for monsoon variations in the context of global-scale climate forcings is critical for foreseeing, and possibly avoiding such disasters in the future (Held et al. 2005).

Previous studies based on fully-coupled atmosphere-ocean-land models have not fully characterized the physical controls of monsoon variability, because the confluence of simultaneously evolving variables in these models hinders mechanistic understanding. While most studies of precessional

forcing have focused on the climate response over Africa only, Merlis et al. more broadly analyzed the tropical precipitation response in an idealized aquaplanet model with a 5-meter slab ocean, and a comprehensive radiation scheme including some representation of clouds [for details on the model, see Merlis et al. 2013a]. Here, we examine an atmospheric model coupled to a 50-meter slab ocean in terms of both regional and zonal mean precipitation changes to build on the findings from both idealized and fully-coupled modeling studies.

In the present study we investigate the response of the West African monsoon and the zonal mean climate to Holocene orbital forcing. We analyze how the impact of the imposed insolation gradient on tropical rainfall differs from the regional to global scales. Based on an energetic analysis of the tropical circulation, we explain the weakening of the zonal mean tropical circulation despite the increased insolation gradient.

2.3 Experimental Design & Methods

This study compares atmospheric general circulation model simulations (Geophysical Fluid Dynamics Laboratory AM2.1) with modern and 10 ka orbital parameters. The model's land configuration does not feature dynamic vegetation, so associated albedo and soil moisture feedbacks are muted.

We isolate the role of ocean thermodynamics in the climate response to Holocene orbital parameters by considering two sets of simulations: one with prescribed sea surface temperatures (SSTs) and one with a 50-meter slab ocean. In the prescribed SSTs experiment, the distribution of SSTs is set to observational means from the Reynolds OI dataset averaged over the period from 1980-1999. In the 50-meter slab ocean configuration, SSTs interact with the atmospheric forcing. Neither simulation allows for adjustments in the ocean dynamics. When Braconnot et al. 2000 compared a prescribed SST simulation with a fully coupled atmosphere-ocean model, they found that the 6 ka change in ocean heat transport is similar to the change in atmospheric heat transport. We therefore anticipate that adjustments to the atmospheric dynamics will be stronger than they would be in a world where both oceanic and atmospheric circulations contribute to poleward fluxes of anomalous energy inputs.

We examine the responses of the regional and zonal mean precipitation by calculating the JJA precipitation anomaly between the 10 ka and modern orbital forcing scenarios, for both sets of ocean experiments. We analyze the energetic and dynamical response to 10 ka orbital parameters to interpret the zonal mean precipitation response. This analysis includes calculation of the anomalies in atmospheric heat transport, the Hadley cell circulation, and the gross moist stability. The physical frameworks for each of these phases of analysis are detailed in subsequent sections. In all calculations, averages are taken over a 16 year period following one year of model spin-up. We focus our report on summer (June, July, and August, or JJA) mean results, since this spans the period when the imposed insolation forcing is greatest in the tropics (Fig. 9 on the following page), as well as the onset of the modern West African monsoon season. We consider the data from each season to understand the influence of the altered insolation distribution on the seasonality of SST patterns in the slab ocean experiment.

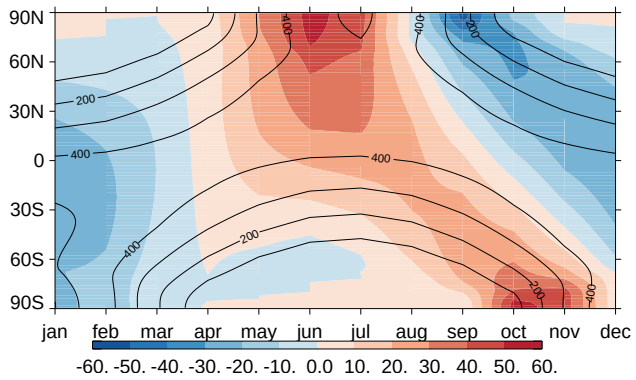

Figure 9: Color contours correspond to the change in downward shortwave radiation (10 ka – Present) at the top of the atmosphere (TOA) (W m^{-2}). Black contours show the values for the present day.

2.3.1 *Atmospheric Heat Transport*

The frozen moist static energy (FMSE) is presented in (6), where C_p is the heat capacity of dry air, T is the temperature in Kelvin, gz is the potential energy, L_v and L_f are the latent heats of vaporization and fusion respectively, and q_v and q_i are the water vapor and ice mixing ratios (Peters et al. 2008).

$$h = c_p T + gz + L_v q_v - L_f q_i \tag{6}$$

The time derivative of the vertical integral of h is equal to the horizontal FMSE flux divergence and the diabatic term Q, as in (7), where a tilde indicates a vertical mass-weighted integral ($\tilde{} \equiv \int \frac{dp}{g}$) (Peters et al. 2008).

$$\frac{\partial \tilde{h}}{\partial t} = -\nabla \cdot (\mathbf{u}\tilde{h}) + Q \tag{7}$$

In moist adiabatic motions, $\tilde{h}$ is conserved, aside from conversions to kinetic energy or contributions from frozen precipitation, both of which are of minimal influence to the energy budget in the tropics (Peters et al. 2008). In our analysis of the tropical energetics, we therefore consider the time derivative of $\tilde{h}$ to be zero, and set the horizontal energy flux divergence equal to the diabatic term Q, as in (8). Q is the difference of the radiative terms and the surface net heat fluxes, which is the effective radiation perturbation that the atmosphere must transport (Merlis et al. 2013b).

Assuming steady state,

$$\nabla \cdot (\mathbf{u}\tilde{h}) = Q = Q_{TOA} - Q_{sfc} \tag{8}$$

The total atmospheric heat transport (AHT) is the the integrated Q as in (9) (Hill et al. 2015). We calculate the total AHT in the 10 ka orbital experiment and the modern control according to (9). We then calculate the anomaly (10 ka - Modern control).

$$F_{tot}(\phi) = \int_{-\frac{\pi}{2}}^{\phi} \int_{0}^{2\pi} (Q_{TOA} - Q_{sfc}) a^2 \cos\phi \, d\lambda \, d\phi \tag{9}$$

2.3.2 *Hadley Circulation*

To ascertain the dynamical mechanism behind the zonal mean rainfall anomaly between the 10 ka and modern control experiments, we calculate the zonal

mean meridional streamfunction for each as in (10), where ϕ is the latitude, p is a pressure height, a is the radius of Earth, $\bar{v}$ is the meridional wind, and g is the acceleration due to gravity.

$$\Psi(\phi, p) = 2\pi a \cos\phi \int_0^p \bar{v}\, dp/g. \tag{10}$$

2.3.3 *Gross Moist Stability*

The total gross moist stability is the ratio of total atmospheric energy transport $F_{tot}(\phi)$ to the mass transport $\Psi(\phi)$ integrated to the pressure height of maximum intensity (Kang et al. 2009). It is calculated as the ratio of fluxes, which is convenient when considering the zonal-mean climate. This form of the GMS is the efficiency of the export of energy by the circulation (Peters et al. 2008). The total gross moist stability is not well defined outside of the equatorial region, beyond the extent of the Hadley cell (Frierson 2007).

We calculated the total gross moist stability and the anomalies for both sets of experiments.

2.4 Results

2.4.1 *Regional Response*

As expected, with both ocean configurations the precipitation increases in the simulations with Holocene parameters, in some places on the order of 100% (Fig. 10). The precipitation increases over West Africa by up to 2-3 mm/day in the prescribed SST case and up to 3-6 mm/day in the slab ocean case. The zonal shift in the rainfall distribution is more dramatic than the meridional shift (Fig 10).

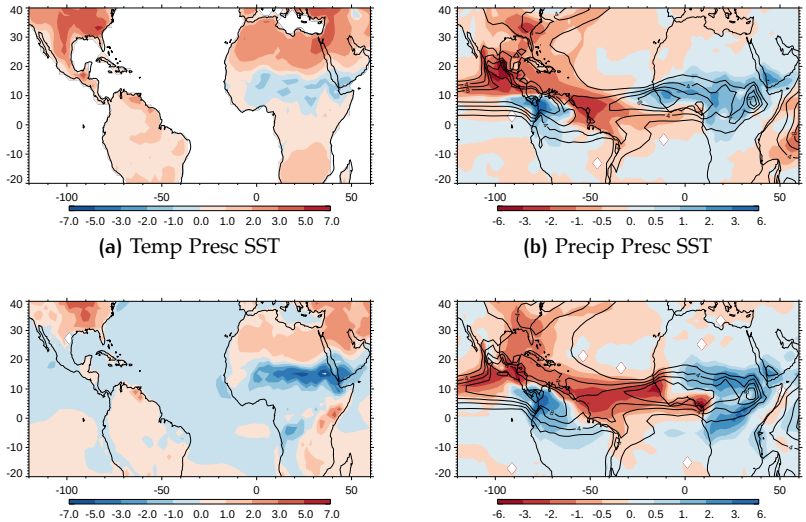

(a) Temp Presc SST **(b)** Precip Presc SST

(c) Temp Slab Ocean **(d)** Precip Slab Ocean

Figure 10: The left panel shows the JJA surface air temperature anomalies (K), and the right panel shows the JJA precipitation anomalies (mm/day). The top row is the prescribed SST experiment, and the bottom row is the slab ocean experiment. Color contours indicate regional temperature and precipitation changes for the prescribed SST and slab ocean experiments. Black contours show the values for the present day.

In a supply-limited evaporative regime such as the Sahel, surface temperature and precipitation are generally tightly anti-correlated due to the impact of rainfall on the surface energy budget (Berg et al. 2015). Precipitation increases soil moisture and latent heat fluxes (enhanced evapotranspiration), and reduces sensible heat fluxes (temperature). As would be expected in a moisture-limited regime over land, JJA temperatures decrease over the Sahel in the 10 ka simulations as precipitation increases, despite the insolation forcing. In the prescribed SST case, the maximum cooling over the Sahel is between 1 and 2 K, and in the slab ocean experiment, the temperature declines over the Sahel by up to 7 K (Fig 10a on the previous page& Fig 10c on the preceding page). In the slab ocean simulation, there are cold Atlantic SST anomalies around the equator during JJA (Fig 10c on the previous page). In the monthly mean temperature anomaly results, we note a seasonal delay in the SST response to the insolation forcing (Appendix,(Fig. 15 on page 33).

The intensification and northward migration of the African monsoon with Holocene precession is evident with both ocean configurations but is stronger in the slab ocean experiment. Both of our experiments underestimate the regional rainfall response compared to paleoclimate proxies (Tierney et al. 2011).

A factor that possibly contributes to the limited northward migration of the West African monsoon in our simulations is the absence of vegetation in the model. Vegetation reduces albedo and increases evapotranspiration, thereby supporting precipitation, and its dynamic response to orbital forcing has contributed substantially to shifts in the monsoon position in other studies (Patricola and Cook 2007). Another important mechanism to consider is ventilation, or the advection of low moist static energy air from the ocean to the continent, which limits the northward extent of monsoons because it is cooler and holds less water vapor, and thus suppresses convection (Hales et al. 2006). It will be worthwhile to compare simulated ventilation with observations or other models to determine if excessive ventilation in the GFDL AM2.1 model inhibits the northward migration of the West African monsoon.

2.4.2 *Zonal Mean Response*

The intertropical convergence zone (ITCZ) is the seasonally migrating band of maximum time-mean precipitation in the tropics (Philander et al 1996). We find that in the 10 ka simulation the ITCZ shifts southward, away from the brighter hemisphere, with both ocean configurations (Fig 11 on the next page). Conventional energetic frameworks would predict the ITCZ to migrate in the opposite direction (Schneider et al. 2014). That we observe this result in the prescribed SST experiment implies that the ITCZ shift is not dictated strictly by seasonal changes to the spatial pattern of SSTs.

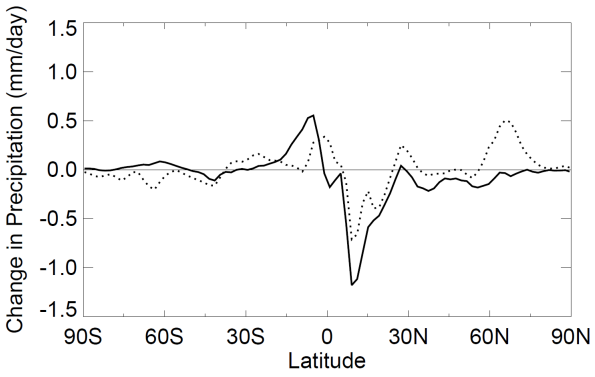

Figure 11: JJA zonal mean δPrecipitation 10 ka – Present. The dashed line corresponds to the prescribed SST simulation, and the solid line to the 50 meter slab ocean simulation.

Our results demonstrate that the imposed JJA insolation change in the 10 ka scenario increases the meridional energy gradient and necessitates a greater southward energy transport (Fig 12). The zonal mean plot of JJA δAHT reveals a peak of southward energy flux of approximately 0.6 Petawatts around 15 degrees North latitude in both the prescribed SST and slab ocean simulations.

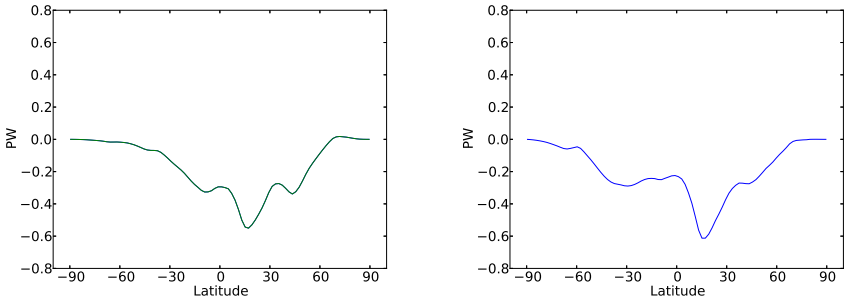

(a) Prescribed SST **(b)** Slab Ocean

Figure 12: Zonally-averaged JJA atmospheric heat transport (AHT) anomaly (10 ka - Modern) in petawatts.

Based on our calculations of the Hadley cell mass flux anomaly, the southward energy flux from the high precession summer hemisphere is not accomplished by a stronger Hadley cell mass flux in either experiment(Fig 13 on the next page). The mass flux does not change appreciably in the prescribed SSTs experiment, and in fact, the circulation weakens in the slab ocean case with a maximum magnitude of 35 - 40 $\times 10^9$ kgs^{-1}(Fig 13b on the following page), over 10 percent of the climatological maximum strength (Fig 13a on the next page).

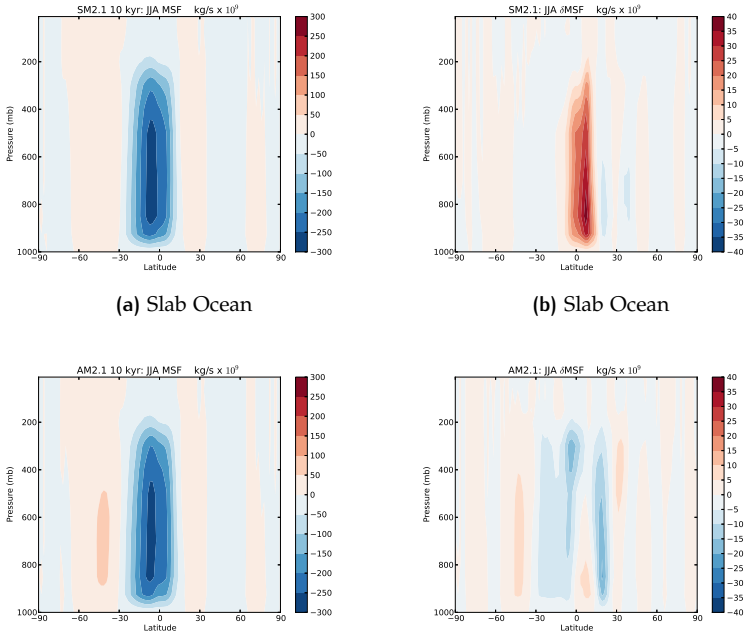

(a) Slab Ocean **(b)** Slab Ocean

(c) Presc SST **(d)** Presc SST

Figure 13: The left panel shows the climatological streamfunction at 10 ka for both ocean configurations. The right panel is the JJA mean δAtmospheric mass transport (meridional streamfunction). Blue values indicate counterclockwise circulation.

We attribute the counterintuitive zonal mean precipitation response to the increase in gross moist stability in the northern tropics in both simulations (Fig 14 on the following page). This increase is greater in the slab ocean experiment, and compensates for the anomalous solar energy input to the NH such that the Hadley cell mass flux decreases, as noted above.

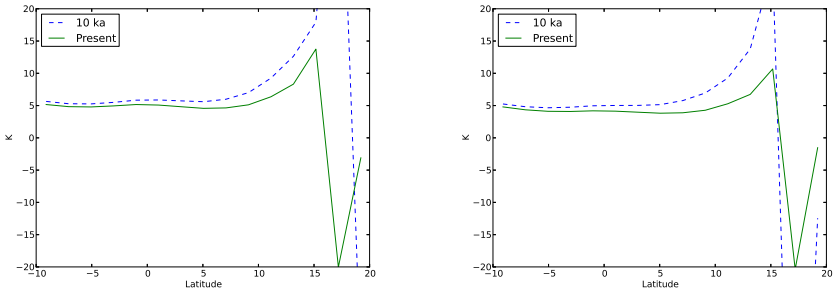

(a) Prescribed SST **(b)** Slab Ocean

Figure 14: Zonal mean JJA gross moist stability for both ocean experiments. The dashed line is the 10 kyr. result, and the green solid line is the present-day GMS.

2.5 Discussion

In both prescribed SST and slab ocean experiments, we report a moistening over Africa accompanied by a counterintuitive zonal mean energetic and precipitation response. This underscores that the basic response of tropical rainfall to Holocene orbital parameters is not dictated by SST changes. The strenghtening of the African monsoon with Holocene orbital parameters is a robust finding in modeling studies across a range of complexities.

The limited northward migration of the monsoon in both simulations presented here emphasizes the importance of processes not represented in the GFDL AM2.1 model, such as the vegetation feedback highlighted by Patricola and Cook (2007). Additionally, due to the 50-meter depth of the slab ocean in our experiment, the ocean thermal inertia is higher than in previous studies. The NH equatorial Atlantic ocean warming due to enhanced summer insolation is delayed to boreal autumn (Fig 15 on page 33). This might limit the northward extension of anomalous JJA rainfall in our study compared to others. The JJA δSST pattern in our slab ocean experiment is inconsistent with what Zhao et al. 2005 observe in a multimodel study of the role of ocean feedback in the enhancement of the African monsoon during the Holocene. They explain an ocean feedback mechanism by which moist inflow over West Africa is favored by a thermal dipole pattern of warm Atlantic SST anomalies around 5 degrees North and cold SST anomalies around 5 degrees South. Braconnot et al. 2012 cite a similar pattern of differential warming as an important ocean feedback that strengthened the African monsoon flow in the Paleoclimate Modelling Intercomparison Project simulations. It is difficult to validate the SST patterns in Holocene model simulations because it is unclear how changes in stratification and seasonality influence the $\delta^{18}O$ composition of foraminifera fossils, which are an important tool in paleo-oceanographic reconstructions (Waelbroeck et al. 2005).

We can gain insight regarding the zonal mean circulation response to orbital precession reported here from the aquaplanet experiment conducted by Merlis et al. 2013a. In this study, an idealized atmospheric model is coupled to a 5-meter deep slab ocean, and the boreal summer Hadley cell mass flux weakens with high precession due to large adjustments of the gross moist stability. As Merlis et al. explain it, the monsoonal Hadley circulation is near the angular-momentum conserving limit, meaning it is energetically

constrained. The moist static energy aloft is nearly uniform given the low water vapor content and two assumptions: a weak temperature gradient in the tropical free troposphere, and a uniform height of the poleward flow (Held 2001). Held posits that the gross moist stability of the Hadley circulation is therefore determined by the horizontal near-surface moist static energy gradient over the meridional extent of the Hadley cell. Based on this, Merlis et al. reason that the Hadley circulation gross moist stability increases in the 10 ka summer because the imposed insolation gradient increases surface moist static energy gradients, while the moist static energy aloft remains uniform. It is interesting that the aquaplanet zonal mean circulation changes are consistent with those in our study, which includes a substantially deeper mixed layer, full continental geometry, and a highly complex representation of the atmosphere. However, in a subsequent paper, Merlis et al. analyze the tropical precipitation response to orbital precession in this aquaplanet experiment, and they find an increase in the zonal mean NH summer precipitation (2013c). Our study finds a similar dynamical response to the Merlis et al. 2013a study, but an inconsistent zonal mean rainfall response with Merlis et al. 2013c. The rainfall changes they describe hold only over land in our study.

In the present study, it is possible that the lag response of the SSTs to insolation and the zonal asymmetries due to continental geometry contribute to the discrepancy with the precipitation changes in Merlis et al. 2013c. Donohoe et al. 2014 report on aquaplanet simulations with varying slab ocean depths. With a 50-meter mixed layer, the ITCZ does not stray as far from the equator into the summer hemisphere as when the mixed layer is shallower (Donohoe et al. 2014). They argue that with a deeper mixed layer, the capacity for ocean storage of insolation inputs increases, reducing temporal SST variability and limiting the latitudinal extent of tropical precipitation.

The opposite responses to orbital precession of the zonal mean and regional tropical precipitation that we report have been noted in only one other study, to our knowledge. In the high-precession climate modeling study by Clement et al. 2004, an atmospheric model is coupled to a 50-meter slab ocean and the ITCZ over land shifts northward, and over ocean shifts southward in boreal summer. We identify several next steps to improve our understanding of this result. Future analysis will investigate whether enhanced zonal advection of moisture from the Atlantic ocean to the African continent is an important process in monsoon strengthening. Additionally, previous studies have explained the way shallow circulations north of monsoon regions can control rainfall variability, and in particular that anomalies in the geopotential low over the Sahara predict rainfall changes over the Sahel (Hurley and Boos 2013; Biasutti et al. 2009). To evaluate whether this process can explain the results we present here, we will assess the shallow circulations associated with the Sahara in our simulations.

A global energetic framework elucidates the zonal mean tropical precipitation response. The change in the efficiency of the atmospheric heat transport compensates for the temporal and spatial adjustments in energy input resulting from Holocene orbital parameters. In the slab ocean experiment, this response eliminates the need for northward migration of the ITCZ. However, even in the prescribed SSTs experiment, the increase in gross moist stability dominates the tropical response to Holocene orbital parameters. We speculate that the zonal mean gross moist stability anomaly might be dominated by the change over land. The roles of the mixed layer depth and the zonal circulation in the precipitation response to Holocene orbital parameters also

warrant further study. Refining our understanding of tropical precipitation dynamics, and particularly monsoon rains, will be crucial for understanding global rainfall patterns in a changing climate.

2.6 Appendix

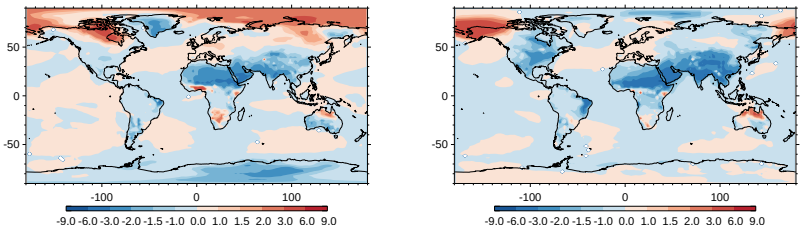

(a) January **(b)** February

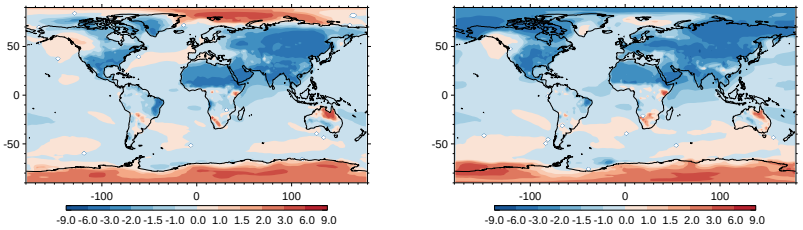

(c) March **(d)** April

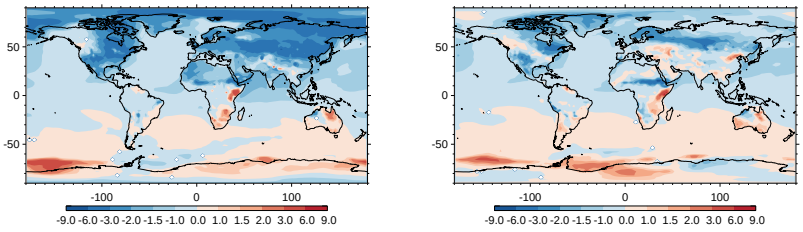

(e) May **(f)** June

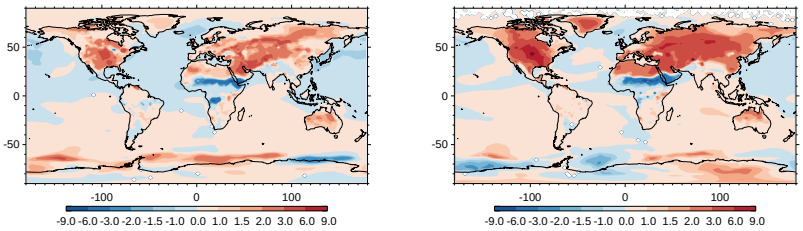

(g) July **(h)** August

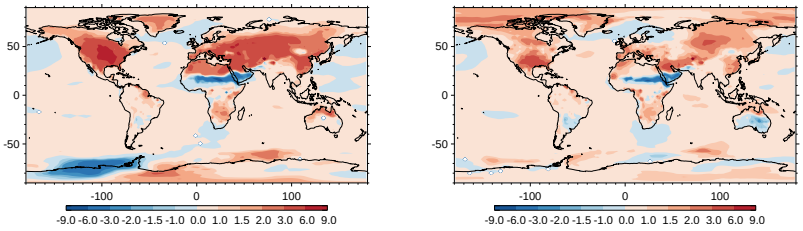

(i) September **(j)** October

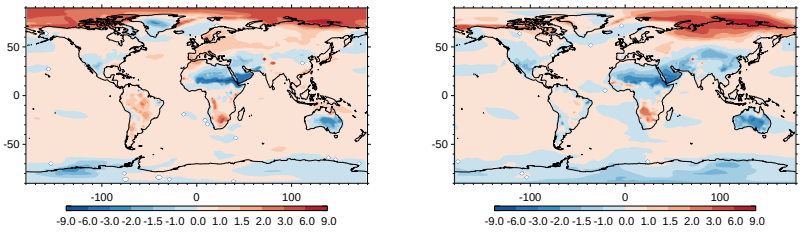

(k) November **(l)** December

Figure 15: The distribution of temperature anomalies (K) between 10 ka and the modern control in the slab ocean model.

REFERENCES

REFERENCES

[*Bala et al.*(2008)] ala et al. (2008), Impact of geoengineering schemes on the global hydrological cycle. *PNAS*, *105*.

[*Berg et al.*(2015)] Berg et al.(2015), Interannual Coupling between Summertime Surface Temperature and Precipitation over Land: Processes and Implications for Climate Change, *J. Climate*, *28*.

[*Biasutti et al.*(2009)] Biasutti et al.(2009),The Role of the Sahara Low in Summertime Sahel Rainfall Variability and Change in the CMIP3 Models, *J. Climate*, *22*.

[*Bosmans et al.* (2012)] osmans et al. (2012), Monsoonal response to mid-Holocene orbital forcing in a high resolution GCM. *Clim. Past*, *8*, 723–740.

[*Braconnot et al.*(2000)] Braconnot et al.(2000), Ocean Feedback in Response to 6 kyr BP Insolation, *J. Climate*, *13*.

[*Braconnot et al.* (2012)] raconnot et al. (2012), Evaluation of climate models using palaeoclimatic data. *Nature Climate Change*, *2*, 417-424.

[*Clement et al.*(2004)] Clement et al.(2004), The importance of precessional signals in the tropical climate, *Clim. Dyn.*, *22*.

[*de Menocal et al.* (2015)] de Menocal et al., (2015), Paleoclimate: End of the African Humid Period. *Nature Geoscience*, *8*, 86-87.

[*Donohoe and Battisti*(2011)] Donohoe and Battisti(2011), Atmospheric and Surface Contributions to Planetary Albedo, *Journal of Climate*, *24*, 4402–4418.

[*Frierson*(2007)] Frierson(2007), The Dynamics of Idealized Convection Schemes and Their Effect on the Zonally Averaged Tropical Circulation, *Journal of the Atmos. Sciences*, *64*.

[*Fyfe et al.*(2013)] Fyfe, J. et al. (2013), Biogeochemical carbon coupling influences global precipitation in geoengineering experiments, *Geophys. Res. Letters*, *40*, 651–655.

[*Hadley*(1735)] Hadley (1735), Concerning the cause of the general trade winds, *Phil. Trans.*, *39*, 58-62.

[*Haywood et al.*(2013)] Haywood et al.(2013), Asymmetric forcing from stratospheric aerosols impacts Sahelian rainfall, *Nature Climate Change*, *March v. 1857*, 1-6.

[*Held*(2001)] Held(2001),The Partitioning of the Poleward Energy Transport between the Tropical Ocean and Atmosphere, *Journal of the Atmospheric Sciences*, *58*, 943–948.

[*Held and Soden)*(2013)] Held and Soden (2000), Water vapor feedback and global warming, *Annual Review of Energy and the Environment*, *25*, 441–475.

[*Held and Soden)*(2006)] Held and Soden (2006), Robust responses of the hydrological cycle to global warming, *Journal of Climate*, *19*, 5686-5699.

[*Held et al.)* (2005)] Held et al., (2005), Simulation of Sahel drought in the 20th and 21st centuries. *PNAS*, *102*, 17891-17896.

[*Hill et al.)* (2015)] Hill et al. (2015), Mechanisms of Forced Tropical Meridional Energy Flux Change, *J. Climate*,*28*.

[*IPCC*(2014)] IPCC (2014), : Climate Change 2014: Impacts, Adaptation, and Vulnerability. Part A: Global and Sectoral Aspects, *Contribution of Working Group II to the Fifth Assessment Report of the Intergovernmental Panel on Climate Change*, [Field, C.B., V.R. Barros, D.J. Dokken, K.J. Mach, M.D. Mastrandrea, T.E. Bilir, M. Chatterjee, K.L. Ebi, Y.O. Estrada, R.C. Genova, B. Girma, E.S. Kissel, A.N. Levy, S. MacCracken, P.R. Mastrandrea, and L.L.White (eds.)]. Cambridge University Press, Cambridge, United Kingdom and New York, NY, USA, 1132 pp.

[*Irvine et al.*(2014)] Irvine et al. (2014),Key factors governing uncertainty in the response to sunshade geoengineering from a comparison of the GeoMIP ensemble and a perturbed parameter ensemble, *Journal of Geophys. Res.: Atmospheres*, *119*, 7946–7962.

[*Joussame et al.*(1999)] Joussame et al. (1999), Monsoon changes for 6000 years ago: Results of 18 simulations from the Paleoclimate Modeling Intercomparison Project (PMIP), *Geophys. Res. Letters*, *26*, 859-862.

[*Kang*(2008)] Kang et al. (2008),The Response of the ITCZ to Extratropical Thermal Forcing: Idealized Slab-Ocean Experiments with a GCM, *Journal of Climate*, *21*, 3521–3532.

[*Kang et al.*(2009)] Kang et al. (2009),The Tropical Response to Extratropical Thermal Forcing in an Idealized GCM: The Importance of Radiative Feedbacks and Convective Parameterization, *Journal of the Atmospheric Sciences*, *66*.

[*Kravitz et al.*(2010)] Kravitz, B. et al. (2010), *Specifications for GeoMIP experiments G1 through G4, Available online*.

[*Kravitz et al.*(2013a)] Kravitz et al. (2013a),Climate model response from the Geoengineering Model Intercomparison Project (GeoMIP), *JGR: Atmospheres*, *118*, 8320–8332.

[*Kravitz et al.*(2013c)] ravitz B., et al. (2013b) An energetic perspective on hydrological cycle changes in the Geoengineering Model Inter-Comparison Project, *JGR: Atmospheres*, *118*.

[*Luan et al.*(2012)] Luan et al. (2012), Early and mid-Holocene climate in the tropical Pacific: seasonal cycle and interannual variability induced by insolation changes, *Climate of the Past*, *2012*, 1093–1108.

[*Merlis et al.* (2013a)] erlis et al., (2013a), Hadley circulation response to orbital precession. Part I: Aquaplanets. *J. Climate*, *26*, 740-753.

[*Merlis et al.* (2013b)] erlis et al., (2013b), Hadley circulation response to orbital precession. Part II: Subtropical continent. *J. Climate*, *26*, 754-771.

[*Merlis et al.* (2013c)] erlis et al., (2013c), The tropical precipitation response to orbital precession. *J. Climate*, *26*, 2010-2021.

[*Neelin and Held* (1987)] eelin and Held, (1987), Modeling tropical convergence based on the moist static energy budget. *Mon. Wea. Rev.*, *115*, 3-12.

[*Nicholson et al.*(2013)] Nicholson et al. (2013), The West African Sahel: A Review, *ISRN Meteorology*, *2013*.

[*NRC*(2015] NRC (2015),"Front Matter." National Research Council. Climate Intervention: Reflecting Sunlight to Cool Earth, Washington, DC: The National Academies Press, 2015. doi:10.17226/18988.

[*Patricola and Cook* (2007)] atricola and Cook, (2007), Dynamics of the West African monsoon under mid-Holocene precessional forcing: Regional climate model simulations. *J. Climate*, *20*, 694–716.

[*Peixoto and Oort*(1996)] Peixoto and Oort(1996),The climatology of relative humidity in the atmosphere, *Journal of Climate*, *9*, 3443–3463.

[*Peters et al.*(2008)] Peters et al. (2008), Analysis of Atmospheric Energy Transport in ERA-40 and Implications for Simple Models of the Mean Tropical Circulation, *Journal of Climate*, *21*.

[*Philander et al.*(1996)] Philander et al. (1996), Why the ITCZ is mostly north of the equator, *Journal of Climate*, *9*, 2958–2972.

[*Prive and Plumb*(2007)] Prive and Plumb (2007),Monsoon Dynamics with Interactive Forcing. Part I: Axisymmetric Studies, *Journal of the Atmospheric Sciences*, *64*.

[*Raymond et al.* (2009)] aymond et al., (2009), The Mechanics of Gross Moist Stability. *J. Adv. Model. Earth Syst.*, *1*, 1-20.

[*Robock et al.*(2009)] Robock et al. (2009),Benefits, risks, and costs of solar geoengineering, *Geophysical Research Letters*, *36*.

[*Schneider et al.*(2014)] Schneider et al. (2014),Migrations and dynamics of the intertropical convergence zone, *Nature Review*, *513*, 45–53.

[*Seo et al.*(2014)] Seo et al. (2014),Sensitivity of Intertropical Convergence Zone Movement to the Latitudinal Position of Thermal Forcing, *Journal of Climate*, *27*, 3035-3042.

[*Schneider et al.*(2014)] Shekhar and Boos (2016),Improving Energy-Based Estimates of Monsoon Location in the Presence of Proximal Deserts, *Journal of Climate*.

[*Stephens et al.*(2015)] Stephens et al. (2015), The albedo of Earth, *Reviews of Geophysics*, *53*, 141–163.

[*Tierney et al.*(2011)] Tierney et al. (2011), Model, proxy and isotopic perspectives on the East African Humid Period, *Earth and Planetary Science Letters*, *307*, 103–112.

[*Voigt et al.*(2013)] Voigt et al. (2013), The observed hemispheric asymmetry in reflected shortwave irradiance, *Journal of Climate*, *26*, 468–477.

[*Waelbroeck et al.*(2005)] Waelbroeck et al. (2005), A global compilation of late Holocene planktonic foraminiferal delta18O: relationship between surface water temperature and delta18O, *Quaternary Science Reviews*, *24*, 853–868.

[*Yoshimori and Broccoli*(2008)] Yoshimori and Broccoli (2008), Equilibrium Response of an Atmosphere–Mixed Layer Ocean Model to Different Radiative Forcing Agents: Global and Zonal Mean Response, *Journal of Climate*, *21*, 4399–4423.

[*Yu et al.* (1998)] u et al. (1998), Estimating the Gross Moist Stability of the Tropical Atmosphere. J. Atmos. Sci., *55*, 1354-1372.

[*Zhao et al.*(2005)] Zhao et al. (2005), A multi-model analysis of the role of the ocean on the African and Indian monsoon during the mid-Holocene, *Climate Dynamics*, *25*, 777-800.